Structural Variability of Nucleosomes Detected by Single-Pair Forster Resonance Energy Transfer: Histone Acetylation, Sequence Variation, and Salt Effects

ARTICLE *in* THE JOURNAL OF PHYSICAL CHEMISTRY B · NOVEMBER 2008

Impact Factor: 3.3 · DOI: 10.1021/jp7114737 · Source: PubMed

4 AUTHORS, INCLUDING:

Katalin Tóth
German Cancer Research Center
58 PUBLICATIONS **951** CITATIONS
SEE PROFILE

Nathalie Schwarz
German Cancer Research Center
3 PUBLICATIONS **49** CITATIONS
SEE PROFILE

Jörg Langowski
German Cancer Research Center
246 PUBLICATIONS **6,443** CITATIONS
SEE PROFILE

Structural Variability of Nucleosomes Detected by Single-Pair Förster Resonance Energy Transfer: Histone Acetylation, Sequence Variation, and Salt Effects†

Alex Gansen, Katalin Tóth, Nathalie Schwarz, and Jörg Langowski*

Division Biophysics of Macromolecules, German Cancer Research Center, Im Neuenheimer Feld 580, D-69120 Heidelberg, Germany

Received: December 5, 2007; Revised Manuscript Received: February 26, 2008

Nucleosomes were reconstituted from 170 bp long fragments of 5S rDNA and an optimal positioning sequence, the Selex 601, with recombinant histones. In free-solution single pair Förster resonance energy transfer (spFRET) measurements of the distance between fluorescently labeled bases in the nucleosomal DNA, the samples exhibited structural diversity. The structural heterogeneity correlated with the stability of the complexes and depended on the DNA sequence and histone acetylation. The stability of the nucleosomes was assessed via dilution-driven disruption: histone acetylation decreased nucleosome stability. The spFRET experiments used a new approach for data acquisition and analysis that we term "deliberately detuned detection" (D^3). This permits the separation of subpopulations in the samples even for the low-FRET regime characteristic for the linker-DNA labeled nucleosomes. Thus, it became possible to study in more detail histone acetylation- and salt-dependent structural variations using either end- or internally labeled DNAs on the nucleosome. We found that the distance distribution of the fluorophore pairs on the linker DNA ends was much more sensitive to histone acetylation or sequence variation than that of labels on the internal part of the DNA, which was more tightly associated with the histone core. spFRET on freely diffusing nucleosomes allows us therefore to localize the influence of histone modifications and DNA sequence variations on the nucleosome structure and dynamics.

Introduction

Gene activity is controlled by the accessibility of chromatin and determined by its structure and stability, which varies locally and temporally. Sequence and chemical modifications of the DNA histone content and posttranslational modifications are responsible for changes in activity and exert their action through the structure of the elemental unit: the nucleosome. Nucleosomes, earlier simply seen as uniform units of compaction, nowadays unfold their structural and functional diversity.

Global−local structure coupling is a central theme in genome structure. Early on, Schurr postulated that superhelical DNA can undergo cooperative structural transitions that may mediate long-range regulatory effects;[1] furthermore, the folding of topologically constrained DNA can lead to global structural changes induced by local bending.[2,3] Such effects may be even more pronounced in a folded nucleosome chain where the global conformation of the chromatin fiber strongly depends on the local geometry of the linker DNA. One very obvious evidence is the opening of the chromatin structure upon the loss of linker histone H1,[4] but also in simulations using the two-angle model for the chromatin fiber, a strong dependence of chromatin structure upon local nucleosome geometry is evident.[5−8] This implies a dynamic view of the DNA on the nucleosome (as evidenced in earlier work by Wang et al.[9] and Schurr & Schurr[10]), which is crucial for such structural changes and for any nucleosome repositioning mechanism.[11] A central problem for the conformational control of chromatin is how histone tail acetylation, other modifications, and electrostatic effects influence the linker DNA geometry. Histone acetylation seems to be correlated with increased genetic activity and hyperacetylation sometimes with cancer; however, the structural basis of the effect is not known yet. Neither are the exact path and DNA contacts of the histone tails known, but it has been shown that without tails no correct chromatin compaction occurs.[12] Histone tails may play a role in the nucleosome−nucleosome interaction either directly or through the linker DNA. Since lysine charges are neutralized upon acetylation, it is plausible that these interactions are weakened and the chromatin structure opens locally, allowing access for different enzymes and transcription machines. Whether charge neutralization alone can induce the observed biological effects has not been analyzed yet; however, it is very likely that the structural effect of histone acetylation is mediated to a large extent by the changes in electrostatic interaction. This view is corroborated by the many observations of the sensitivity of chromatin structure to salt concentration. Compact and open chromatin fibers may be interconverted by varying the type and concentration of monovalent and divalent salts.[4] All these results imply salt-induced closing of the linker DNA arms in oligonucleosomes.

In a previous study, we used Förster resonance energy transfer (FRET)[13] between fluorophores attached to the two ends of a mono- or trinucleosomal DNA in order to quantitate changes in linker DNA geometry upon histone acetylation and changes in salt concentration.[14−16] These measurements, which were done in bulk fluorimetry, suggested that the linker DNA arms in mononucleosomes diverge slightly as they leave the histone core surface. That hypothesis was later confirmed by the crystal structure of the tetranucleosome.[17] Histone H1 led to a global approach of the linker DNA arms, confirming the notion of a stem structure.[18] Increasing salt concentration also led to an approach of the linker DNAs. Acetylating all histones, or selectively H3, caused an opening of the nucleosome structure, indicated by larger distances between the linker DNA ends.

† Part of the "J. Michael Schurr Special Section".

* Corresponding author. E-mail: jl@dkfz.de.

10.1021/jp7114737 CCC: $40.75
Published on Web 10/25/2008

Selective acetylation of H4, however, opened the linker ends for short fragments but caused an approach for fragments longer than 180 bp.[15]

Although the bulk FRET studies gave valuable insight into the mononucleosome structure and its variations, they only yielded an average donor-to-acceptor distance (time-resolved fluorimetry could give somewhat more information through lifetime distributions, but the resolution is limited). An intriguing improvement that has been developed over the past few years is the measurement of FRET on individual particles, or "single pair FRET" (spFRET).[19−23] It has been applied both to immobilized molecules and to those free in solution. Its unique ability to resolve static and dynamic heterogeneities within the sample and the lack of need for synchronization make spFRET the method of choice for investigating nucleosomal dynamics and structural diversity. Single-pair FRET on surface-tethered nucleosomes was used to unravel spontaneous fluctuations of their structure.[24,25] The possibility of detecting single nucleosomes in solution, using observation in a microscope with confocal optics, has been demonstrated,[26] and we recently studied the optimum conditions for detecting spFRET on nucleosomes and showed the resolution of structural subpopulations.[27]

One major difficulty in spFRET measurements of end-labeled nucleosomes is that the relevant distances are all larger than typical Förster radii of 5−6 nm, thus FRET efficiencies are generally low. Since FRET efficiencies are obtained from a rather low number of photon counts in two color channels during the passage of a particle through the focus, they can usually be resolved only over a rather small dynamic range of FRET efficiencies. However, low-FRET events may be artificially "enhanced" by increasing the detection efficiency in the acceptor channel relative to that of the donor. We show here that such "deliberately detuned detection" (D^3) can increase the resolution for low-FRET samples, e.g., by separating them from the contribution of free DNA that may have dissociated from the histone core during the experiment.

Here we applied these techniques together with the stabilization conditions developed earlier[27] for studying the effect of DNA sequence, histone acetylation, and salt conditions on mononucleosome structure. We used nucleosome populations reconstituted on 170 bp DNA fragments containing the 5S rDNA nucleosome positioning sequence from *Xenopus borealis* or the SELEX-generated 601 sequence described by Thastrom et al.[28] The donor and acceptor fluorophores were either at the linker DNA or at internal labeling positions. The nucleosomes were reconstituted from the DNA and recombinant histones by salt dialysis, and the effect of acetylation was studied by acetylating the histones chemically by incubation with acetyl phosphate. Comparing nucleosomes labeled on the internal parts of the DNA with those carrying the label on the linker arms, we could show that the structural effect of histone acetylation is primarily on the outer parts of the linker DNA.

Theoretical Aspects

Resonance energy transfer between two fluorophores is a powerful tool to measure nanometer distances on the molecular level. An induced dipole−dipole interaction leads to transfer of excitation energy from the donor molecule to a nearby acceptor with a distance-dependent efficiency given by

$$E = \frac{1}{1 + (R/R_0)^6} \tag{1}$$

where R_0 is the Förster radius of the fluorophore pair, i.e., the distance at which 50% energy transfer occurs. Most fluorophore pairs have a Förster radius around 5.5−6 nm, which allows measuring distances between 2.5 and 10 nm, matching the scale of a mononucleosome.

Single-molecule FRET efficiencies are calculated from the number of photons detected in the donor and acceptor channel. These signals contain additional contributions from background, direct acceptor excitation, and donor crosstalk into the acceptor channel. Separate measurements on a donor-only sample determine the crosstalk factor α_{DA}, which is given by the intensity ratio of the acceptor signal to the donor count rate. The background rates B_D and B_A for the donor and acceptor channel are obtained from the count rate of the pure buffer solution. The contribution of the direct acceptor excitation is determined from a double labeled sample with $R_{DA} \gg 10$ nm, e.g., a long (170 bp) DNA fragment. After correcting the count rates for crosstalk and background, the direct excitation is given by the excess signal in the acceptor channel.

For each individual burst, the FRET efficiency E is calculated as

$$E = \frac{N_A}{N_A + \gamma N_D} \tag{2}$$

where $\gamma = \eta_A\Phi_A/\eta_D\Phi_D$ is the *detection factor* of the system, composed of the detection efficiencies of both channels, η_D and η_A, and the quantum yields of the fluorophores, Φ_D and Φ_A. The background- and crosstalk-corrected photon numbers, N_A and N_D, are given by

$$\begin{aligned} N_A &= \left(N_A^{(k)} - B_A d^{(k)}\right) - \alpha_{DA}\left(N_D^{(k)} - B_D d^{(k)}\right) \\ N_D &= \left(N_D^{(k)} - B_D d^{(k)}\right) \end{aligned} \tag{3}$$

$N_D^{(k)}$ and $N_A^{(k)}$ are the uncorrected photon counts in the donor and acceptor channel for the kth single molecule event. $d^{(k)}$ is the corresponding duration of the event, and B_D and B_A are the background count rates determined from the buffer solution.

Proximity Ratio vs FRET Efficiency. The detection factor γ needs to be known precisely to interpret the measured photon numbers correctly into a FRET efficiency and interfluorophor distance. This factor is difficult to determine under single molecule conditions and one-color excitation, and additional ensemble data are required. Fortunately, even without exact knowledge of γ, the ratio of the photon counts in both channels already provide information on the heterogeneity in the sample. This is analyzed in terms of the *proximity ratio P*

$$P = \frac{N_A}{N_A + N_D} \tag{4}$$

In particular, if only relative changes in the histogram are of interest, both quantities should provide comparable results. The proximity ratio is closely related to the FRET efficiency, and both quantities can be transformed into each other according to

$$P = \frac{\gamma}{\gamma - 1 + 1/E} \tag{5}$$

The mutual relation between both quantities is plotted in Figure 1 for various values of γ.

Three different regimes can be distinguished:

1. For $\gamma < 1$, a given interval of low FRET efficiencies translates into a smaller proximity ratio range, and two populations with low FRET are less separated in their proximity ratios. High-FRET states, on the contrary, will show an increase in the separation of P values compared to their FRET efficiencies. These settings are convenient for analyzing conformations with fluorophores close to each other.

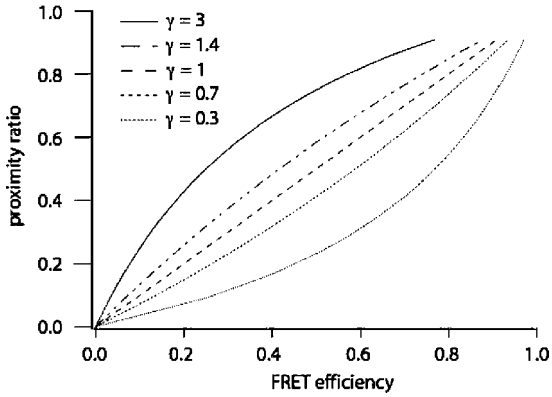

Figure 1. Relation between FRET efficiency and proximity ratio for different detection factors γ.

2. If $\gamma > 1$, two states with low FRET become more separated in their proximity ratios, while at high FRET values, the opposite is observed. This regime is advantageous for the analysis of low-FRET samples, such as linker DNA labeled nucleosomes.

3. For $\gamma = 1$, the proximity ratio equals the FRET efficiency, and no increase/decrease in separation is achieved.

FRET Distribution Width and Shot Noise Limit. Once the energy transfer or proximity ratio is determined for each molecule, a histogram of the calculated quantities reveals the presence of any heterogeneity in the ensemble. Each subconformation appears as a more or less distinct peak in the distribution function.

Even a sample in which all molecules have exactly the same energy transfer will show a broadened peak in the corresponding single molecule histogram. The corresponding width ΔE is a consequence of the photon counting statistics and is determined by the shot noise in the system. It is a function of the mean energy transfer m_E, the detection factor γ, and the detected photon number $S = N_A + N_D$.

To estimate the effect of γ on the shot noise-determined width, we approximate ΔE by the sum of variances in the donor and acceptor counts.[29]

$$(\Delta E)^2 = \left(\frac{\partial E}{\partial N_A}\right)^2 (\Delta N_A)^2 + \left(\frac{\partial E}{\partial N_D}\right)^2 (\Delta N_D)^2 \qquad (6)$$

The number of detected photons can be described by Poissonian statistics, and the respective standard deviations correspond to the square root, $\Delta N_{A/D} = (N_{A/D})^{1/2}$

$$\Delta E = \left[\frac{\gamma}{(1+\gamma N_D/N_A)^2}\right] \cdot \sqrt{\left(\frac{N_D}{N_A^2}\right)\left(\frac{N_D}{N_A}\right) + 1} \qquad (7)$$

For a mean energy transfer m_E, the detected acceptor and donor counts, N_A and N_D, are related by $N_D = N_A(1 - m_E)/\gamma m_E$. For a total number of S detected photons, we can write $N_A = S \cdot (1 + (1 - m_E)/\gamma m_E)^{-1}$ and reformulate ΔE in terms of m_E and S

$$\Delta E = m_E(1 + m_E(\gamma - 1))\sqrt{\left(\frac{1-m_E}{\gamma m_E}\right)\frac{1}{S}} \qquad (8)$$

The analogous expression for the proximity ratio is given by

$$\Delta P = \frac{\gamma}{(\gamma - 1) + 1/m_E}\sqrt{\left(\frac{1-m_E}{\gamma m_E}\right)\frac{1}{S}} \qquad (9)$$

If $\gamma = 1$, eqs 8 and 9 both yield the same result

$$(\Delta E)_{\gamma=1} = \sqrt{\left(\frac{m_E(1-m_E)}{S}\right)} \qquad (10)$$

which is the familiar expression derived in the literature, e.g., Deniz et al.[29] The dependence of ΔE and ΔP on the detection factor γ and the mean energy transfer m_E is shown in Figure 2.

The ratio of both quantities, $\Delta E/\Delta P$, is given by

$$\frac{\Delta E}{\Delta P} = \frac{(1 + m_E(\gamma - 1))^2}{\gamma} \qquad (11)$$

which reduces to unity if $\gamma = 1$.

We note that for small energy transfer m_E and large γ values, ΔP is significantly larger than ΔE, whereas at larger energy transfer and small detection factors, the opposite is observed. The change in shot noise broadening correlates with the increase in separation. For $m_E = 0.2$ and $\gamma = 3$, the relative increase in shot noise is $\Delta P/\Delta E = 1.53$, while $P/E = 2.1$.

Materials and Methods

Preparation of Oligonucleotide Standards. Fluorescently labeled oligonucleotides of 26 base pairs in length were used as FRET standards. Single strand DNAs (5′-*CAAACTAC-CGAGTCTGATACAGGCGC*-3′ and its complementary sequence) were purchased from IBA (IBA Naps, Göttingen, Germany). The fluorophores were attached at position 6 from the 5′ end of each strand via aminolink-dT carbon 6 linkers. The donor fluorophore was Alexa 488, and the acceptor fluorophore was Alexa-568. Donor- and acceptor-labeled strands were hybridized in TE (10 mM Tris-HCl pH 7.5, 0.1 mM EDTA) and 100 mM NaCl. DNA was used at concentrations between 1 and 10 μM. Samples were heated to 95 °C to melt any prehybridized strands and slowly cooled down to room temperature for about 2 h. Samples were then stored in the hybridization buffer at 4 °C and were stable for several months.

Preparation of Labeled Mononucleosomes. The preparation of mononucleosomes followed a protocol similar to that reported in previous work from our group.[14,15,27] Double-labeled 170 base pair long DNA fragments were prepared by preparative PCR using the Selex601 sequence contained in the plasmid templates pgem3z601 (kindly provided by Jon Widom, Northwestern University) and the 5S rDNA gene o*f Xenopus borealis*. The known positioning centers were also the centers of the fragments. The donor fluorophore was Alexa 488; the acceptor fluorophore was Alexa-594; and labeled primers were purchased from IBA Naps, Göttingen. The fluorophore position was varied in order to label different parts of the nucleosomal DNA, namely, the linker DNA at both ends $5S^{end}$ 601^{end} and internal DNA sites 93 base pairs apart $5S^{int}$ 601^{int}, which positioned them close to each other and opposite to the dyad axis in the folded nucleosome. These labeling positions were chosen so that conformational changes in different regions of the nucleosome could be monitored. The different labeling positions are schematically shown in Figure 3.

DNA fragments (0.5 μM) were mixed with recombinant untreated or chemically acetylated histone octamers (prepared as described earlier[15]) at 2 M NaCl-TE buffer and reconstituted into nucleosomes by dialysis in a slowly decreasing salt gradient down to 5 mM NaCl. The molar ratio of the DNA:octamer mixture was optimized between 1:1.3 and 1:2 for each DNA to avoid aggregation and minimize excess free DNA. The quality of nucleosomes was controlled by gel electrophoresis on 2% agarose gels in 0.5 × TBE buffer at a field strength of 10 V/cm and by bulk spectroscopic measurements. Samples containing aggregates or more than 15% free DNA were excluded. For

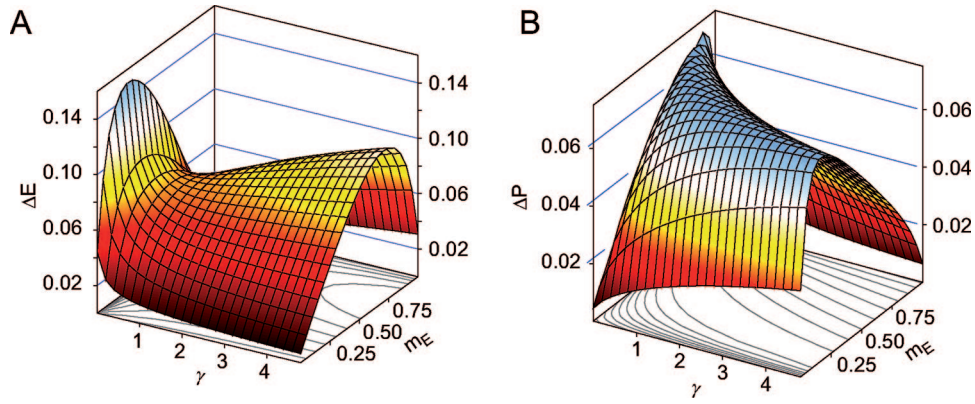

Figure 2. Shot noise limited distribution width of the energy transfer (panel A) and the proximity ratio (panel B) as a function of the mean energy transfer of the molecule, m_E, and the detection factor γ. Data were calculated for a threshold of $S = 50$ photons per burst.

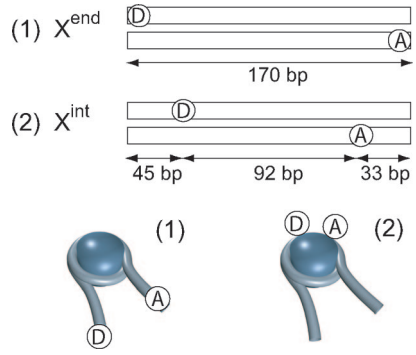

Figure 3. Fluorophore position on the DNA for the different nucleosome constructs used in this study.

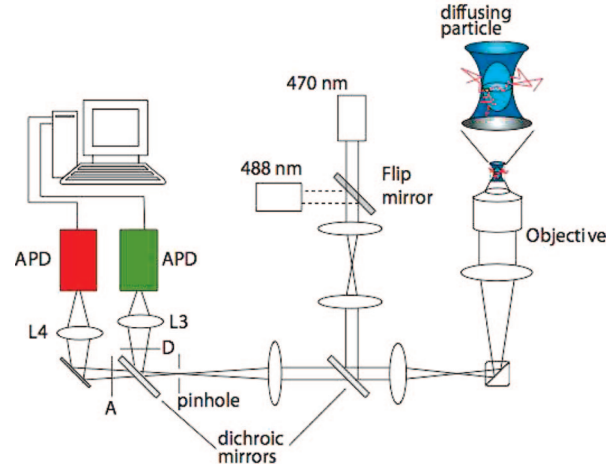

Figure 4. Experimental setup used for the detection of individual nucleosomes in solution.

the single molecule measurements, the nucleosomes were diluted into TE buffer containing 5−100 mM NaCl. To minimize effects of photodestruction and adsorption on the chamber walls (uncoated μ slides Ibidi, München, Germany), the measurements were done in the presence of 1 mM ascorbic acid, 5 mM β-mercaptoethylamine, and 0.1 mg/mL bovine serum albumin.[27] Unlabeled mononucleosomes were prepared from HeLa cell nuclei[30] and added at 10−20 nM concentration in some samples to avoid unfolding. Samples were equilibrated for a minimum of 30 min in the measuring chamber. For thermal mobilization experiments, the nucleosome stock solution was incubated at 5 mM NaCl for 2 h at 55 °C and cooled back quickly to room temperature.

Experimental Setup. Experiments were performed in a setup of our own construction, in which an inverted microscope was supplemented with confocal excitation and detection optics. The overall system is similar to that used in previous work from our group [27,31,32] with modifications introduced into the excitation beam path. Figure 4 shows a schematic view. Donor excitation was done either with a pulsed laser diode at 470 nm (Picoquant GmbH, Berlin, Germany) or a continuous-wave Ar/Kr laser at 488 nm (Melles Griot, Darmstadt, Germany). The beam diameter was reduced by telescope optics to underfill the back focal aperture of a high NA objective lens, producing an enlarged focal spot size. A dichroic mirror (505DRLP) separated the fluorescence from the residual Rayleigh scattering of the laser light and imaged the fluorescence onto the aperture of a 100 μm pinhole located in a conjugated image plane of the objective. The transmitted fluorescence was split into two spectral windows as defined by a replaceable filter unit that housed a dichroic beam splitter (580DRLP) and appropriate interference filters. For establishing deliberately detuned detection (see below), several filters were compared, which are denoted as follows: donor channel, "D^{wide}", 535AF45, "D^{narrow}", 535DF35; acceptor channel, "A^{wide}", OG590/700CFSP, "A^{narrow}", 635DF55, all from Omega Optical. A lens in front of each detector focused the fluorescence onto the active area of the photodiode.

Data Analysis. The single photon data stream from the detectors was read out by a TCSPC board (TimeHarp200, Picoquant GmbH, Berlin, Germany). A software developed in our group discriminated single molecule events against the background signal, based on the time difference between two successive photons as described by Eggeling et al.[33] These interphoton times were smoothed by an LEE filter[34] to reduce the effect of noise in the signal. For each photon, the interphoton time was averaged over ≈15 neighboring photons. The subsequent burst selection algorithm only accepted those events where at least 50 photons were detected with a time separation less than 100−120 μs. The exact thresholds were set by visual inspection of the filtered interphoton time trace.

For each registered event, several burst parameters were calculated, such as its duration, burst size, and in-burst photon rate. The latter was given as the burst size divided by the burst duration. These parameters aided to discriminate further against multiparticle events as described by Gansen et al.,[27] since for an individual molecule a larger burst size in general correlates with increased burst duration. Large deviations from this dependence indicated potential multiparticle events, which were discarded from further analysis.

The distribution of interfluorophore distances was analyzed in terms of the proximity ratio defined in eq 4. Subpopulations

in the histogram were approximated by Gaussian distributions where possible. The corresponding center peak position was converted into a FRET efficiency value according to eq 5. The detection factor γ was estimated from the quantum yields, which were determined from ensemble fluorimetry and the transmission profiles of the filters.

Results and Discussion

To obtain a complete picture of nucleosome dynamics, structural changes must be monitored at several different DNA loci in the complex. In particular, one needs to compare sites in the linker DNA arms with internal sites, where the DNA is attached to the octamer core. So far, all single molecule experiments reported were done on internally labeled DNA sites, which offer a well-detectable FRET efficiency of up to 80%.[24−27,35] Fluorophores attached to the linker DNA, in contrast, only provide average FRET efficiencies of less than 30−35%,[15] a range that is difficult to resolve in diffusion-based experiments. The resolution of subpopulations in this low-FRET regime is limited by the omnipresent zero-FRET peak, which is caused by inactive or missing acceptor species. A second contribution at zero FRET arises from free DNA, either as a remnant of the preparation or dissociated from previously intact nucleosomes. It has been shown in our previous spFRET experiments[27] and in other studies[36,37] that this contribution is not negligible under nucleosome concentrations below its natural dissociation constant. Here, the increasing proportion of free DNA complicates the analysis of low-FRET events, since the distribution width of the zero-FRET peak increases significantly (up to 50%) compared to an equivalent donor-only labeled sample. This additional broadening is at least partially caused by the direct excitation of the acceptor fluorophore. To improve the dynamic range in which low-FRET subpopulations can be distinguished from the zero-FRET peak and analyzed with one-color excitation, we increased the detection factor in a controlled way by reducing the donor detection efficiency through deliberately detuned detection (D^3). The principle of this approach is described in the following.

Deliberately Detuned Detection (D^3). The distribution of interfluorophore distances can be analyzed in terms of either the FRET efficiency E or the proximity ratio P. For many experiments, only relative changes within the histogram are of interest, so both quantities should yield comparable results. Setting the detection factor γ (see above) to a value >1 renders the optical system more sensitive to the low-FRET region, where the separation on the proximity ratio scale is increased. At the same time, the shot noise-induced peak width is also enlarged. Both counteracting effects determine the value of γ for an optimum separation of end-labeled nucleosomes.

The detection factor can be varied by manipulation of the detection efficiencies of the donor and acceptor channel, η_D and η_A. In general, the efficiency with which a photon from fluorophore i is detected in channel j, η_{ij} (i,j: donor, acceptor) can be factorized into a spectral component, η_{ij}^{spec}, and a geometry-dependent term η_{ij}^{geom}

$$\eta_{ij} = \eta_{ij}^{geom} \cdot \eta_{ij}^{spec} \quad (12)$$

The spectral term depends on the overlap of the emission spectrum of the fluorophore with the transmission profiles of the optical elements and the spectral sensitivity of the avalanche photodiode. The geometric term includes all wavelength-independent contributions, e.g., the collection efficiency of the objective lens (≈ 0.25), and is particularly sensitive to the alignment of the lenses L3 and L4 in front of the detectors (see Figure 4).

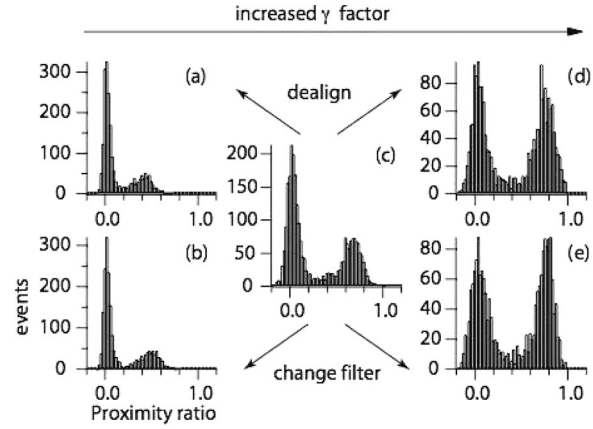

Figure 5. Comparison of the two methods to manipulate the detection factor γ. Starting from the filter combination $D^{wide}A^{wide}$ (c) the detection factor was lowered by (a) detuning the acceptor channel or (b) replacing A^{wide} by A^{narrow}. Correspondingly, γ was increased by (d) detuning the donor detection channel or (e) replacing filter D^{wide} by D^{narrow}.

TABLE 1: Detection Factors γ, Measured Proximity Ratios P_{exptl}, and Calculated Transfer Efficiencies E_{calcd} of the High-FRET (E_{calcd} = 0.65) Standard for Different Filter and Alignment Conditions[a]

filter	γ	P	E
D^{wide} A^{narrow}	0.41	0.460 ± 0.007	0.676 ± 0.027
$D^{wide}(A^{wide})$*	0.35	0.384 ± 0.005	0.654 ± 0.021
D^{narrow} A^{narrow}	0.56	0.543 ± 0.011	0.686 ± 0.023
(D^{wide})*(A^{wide})*	0.64	0.504 ± 0.008	0.614 ± 0.020
$D^{wide}A^{wide}$	1.2	0.653 ± 0.005	0.631 ± 0.022
$D^{narrow}A^{wide}$	1.82	0.745 ± 0.009	0.619 ± 0.025
(D^{wide})*A^{wide}	1.66	0.738 ± 0.006	0.629 ± 0.022

[a] The asterisk marks the conditions where the corresponding detection path has been dealigned.

The spectral component can be varied by using different emission filters. This generally requires realignment, which is rather time-consuming. A more reproducible procedure is to change the geometric detection efficiency by deliberately misaligning the lenses L3 and L4.

Both strategies are depicted in Figure 5, where a mixture of donor-only (E = 0) and high-FRET standards (E = 0.65), labeled with Alexa488 and Alexa568, was analyzed under different γ settings. Starting from conditions where $\gamma \approx 1.2$ (filter set $D^{wide}A^{wide}$), either the geometric term η^{geom} was changed by misaligning the optical system (upper histograms, denoted by asterisks in Table 1) or the spectral term η^{spec} was varied by replacing the emission filters (lower histograms, normal notation). Table 1 shows the estimated γ values, the mean proximity ratio, and the calculated FRET efficiency for the high-FRET distribution, calculated by eq 5.

As can be seen from the histograms, an increase in the detection factor γ caused a significant increase in the separation between the two populations. Under conditions where the spectral detection windows were changed, the estimated FRET efficiencies showed a significantly larger spread compared to those obtained with misaligned lenses. The estimation of γ, which is required to determine the FRET efficiency, is more robust if the filters are not changed. Replacing the emission filters causes additional uncertainties since the filter quality might change over time due to abrasion or dirt on the optical coatings. Estimating η^{spec} from the original filter transmission

profiles will not account for filter degradation. Furthermore, frequent handling of emission filters is rather inefficient and delicate. Misalignment of the detection pathway for a given filter set virtually produces a continuum of available detection factors. We therefore decided to use a controlled manipulation of the geometric detection efficiencies by detuning the optical system.

We note that increasing the detection factor may distort the results by introducing a decrease in registered donor-only and/or close-to-zero FRET events. This results from the excessively reduced detection probability for photons emitted from the donor. Molecules exhibiting FRET will have a significant emission in the red channel, and their probability of detection is less affected. This bias becomes important at stronger misalignment and restricts the range of useful γ values. From the experience during this work, a factor up to $\gamma = 3$ still yielded reasonable results.

Effect of Nucleosome Concentration. Dissociation of the nucleosome occurs at concentrations of <100 pM,[27,37] the range at which single molecule experiments are usually performed. Generally, this destabilization is enhanced by increasing the salt concentration over 50 mM monovalent salts.[38] Disintegration of the nucleosome reduces the fraction of intact conformations—maybe selectively—and precludes a thorough analysis of low-FRET species, as more free DNA is produced.

For the analysis of nucleosome conformation under quasi-bulk conditions, a considerable nucleosome concentration has to be maintained (>few nM), while true single molecule conditions imply not to use more than 50−100 pM labeled nucleosomes. To combine both contradictory aspects, we increased the total nucleosome concentration by adding an excess of unlabeled nucleosomes to the solution. This minimized the destabilization of nucleosomes at higher salt, as demonstrated by the D^3-spFRET histograms in Figure 6A and B. At 100 mM NaCl, the intact nucleosome population increased significantly for both 601^{end} and 601^{int} complexes. In the absence of unlabeled complexes, only 51.2% of 601^{int} nucleosomes remained intact, while 76.4% intact complexes were observed if 10 nM unlabeled nucleosomes were present in the sample. These observations imply that the stability of nucleosomes can be measured in a controlled way, by simply reducing the concentration of unlabeled nucleosomes. Potential differences in the stability of nucleosomes can then be investigated as a function of histone modification or DNA sequence variation.

Another way to study nucleosome stability is by increasing the temperature. While this approach is often used to assess nucleosome mobility on the ensemble level,[39,40] we found that it caused a considerable nucleosome degradation under single molecule concentrations. The fraction of intact complexes decreased by about 30% if no additional nucleosomes were added (Figure 6C). This could again be prevented by addition of an excess of unlabeled nucleosomes. Full stability was maintained in this case if an excess of 30 nM unlabeled nucleosomes was present (data not shown).

Effect of DNA Sequence and Histone Acetylation. In spFRET measurements under D^3 conditions, we now investigate how structural changes in the DNA and the histone octamer influence the conformational dynamics of the nucleosome. We first compare structural properties of nucleosomes reconstituted with two different positioning sequences, the highly affine 601 sequence and the less strong binding 5S rDNA. Single molecule experiments monitored the distribution of linker DNA conformations as well as those of DNA sites attached to the octamer. The effect of complete histone tail acetylation on the structure of both different nucleosomes was then studied under equivalent

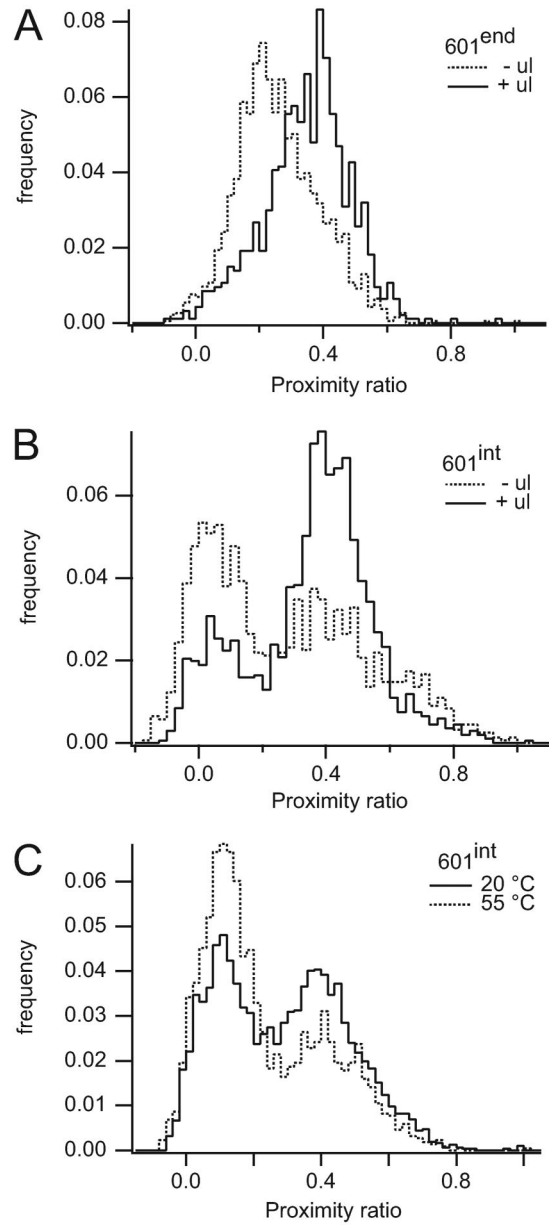

Figure 6. Stability of single nucleosomes. (A) 601^{end} nucleosomes measured in the presence (solid line) and absence (dotted line) of 10 nM unlabeled nucleosomes in 100 mM NaCl. (B) Respective data for 601^{int} nucleosomes in 100 mM NaCl. (C) 601^{int} nucleosomes measured in 10 mM NaCl before (solid line) and after (dotted line) exposure to 55 °C for 2 h in the absence of unlabeled nucleosomes.

quasibulk conditions, where an excess of 10−20 nM unlabeled nucleosomes were added. Finally, the alteration of nucleosome stability as a consequence of the structural change induced by histone acetylation or altered DNA sequence was assessed under highly destabilizing conditions, such as elevated salt concentrations and high nucleosome dilution.

5S and 601 Nucleosomes Differ in Their Structural Heterogeneity. Figure 7 shows D^3-spFRET histograms comparing nucleosomes reconstituted from nonacetylated octamers on 170 bp DNA fragments containing the 601 (dotted lines) and 5S rDNA (solid lines) positioning sequences. The proximity ratio distribution is shown for both linker-DNA-labeled (panel A) and internally labeled nucleosomes (panel B) measured at 100 mM NaCl and a 10 nM excess of unlabeled nucleosomes. The conformational heterogeneity for the linker DNA-labeled nucleosomes is much more pronounced for the 5S sequence. A

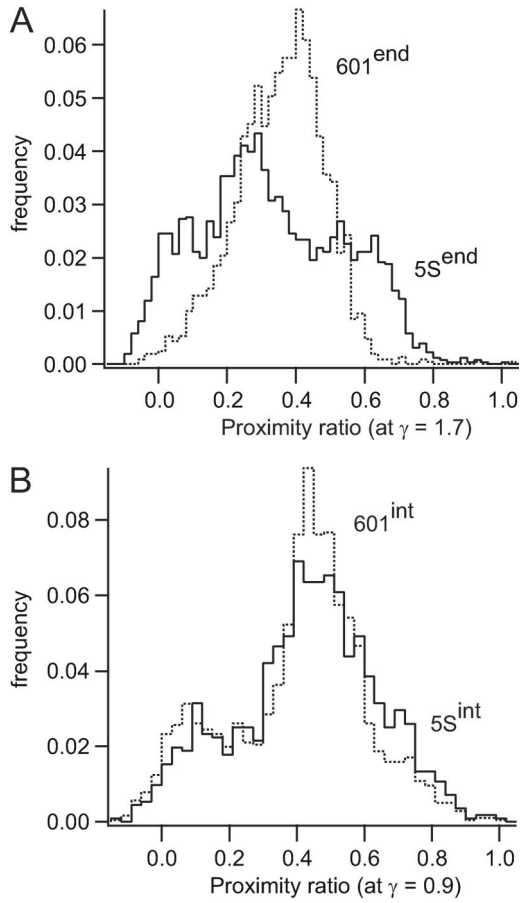

Figure 7. Structural heterogeneity observed for nucleosomes assembled with different DNA sequences. (A) Proximity ratio distribution for end-labeled 5S (solid line) and 601 nucleosomes (dotted line). (B) Respective proximity ratio for internally labeled complexes. All data were acquired in the presence of 10 nM unlabeled nucleosomes.

considerable fraction of complexes was detected with proximity ratios as high as 0.7, suggesting the presence of subconformations where the linker arms of the DNA are in close proximity. 601^{end} nucleosomes, on the contrary, formed a narrow distribution of intact nucleosomes, where a large proximity ratio component was absent.

Only much smaller differences were observed for internal DNA sites: $5S^{int}$ nucleosomes showed a slight broadening of the nucleosome peak compared to 601^{int} constructs. The excess width suggests an increased conformational flexibility of DNA sites in 5S nucleosomes, which is absent in nucleosomes formed with the more affine 601 sequence. These latter appear rather rigid and show a minor second conformation with increased proximity ratio. On the basis of our previous single molecule experiments with the 601 sequence,[27] this second peak might be due to some positioning heterogeneity. In 2% agarose gel electrophoresis (Figure 9), all nucleosome samples, whether reconstituted on the 5S or the 601 sequence, show a minor second band. The relative fraction of this band, however, does not change significantly with DNA sequence of histone acetylation. We therefore attribute the broadening for the 5S sample in Figure 7A to increased dynamics of this sequence as compared to the 601 DNA. Whether the broadened distribution observed for 5S nucleosomes is composed of two or more different substates will be the subject of further investigations.

Histone Acetylation Opens the Outer Regions of Nucleosomal DNA. The effect of histone acetylation was analyzed for both DNA sequences, with an excess of 15 nM unlabeled HeLa nucleosomes. Conformational changes were monitored for the linker DNA portion as well as internal DNA sites. Figure 8 shows D^3-spFRET histograms comparing the effect of acetylation of all histone proteins to unmodified histones at 100 mM NaCl.

The upper two panels of Figure 8 (A and B) show the effect of acetylation on the proximity ratio distribution for DNA labeled at internal sites (for label positions, see Figure 3). Except for a very slight broadening, the histograms for the acetylated and nonacetylated samples are almost superimposable. This indicates that no large structural variations in this part of the nucleosome occur upon histone acetylation. Also, as in Figure 7, the effect is similar for both sequences. However, as the lower two panels of Figure 8 indicate (C and D), nucleosomes with end-labeled DNA are much more affected by histone acetylation than the internally labeled samples. A significant conformational change is induced for both DNA sequences. 601^{end} nucleosomes exhibited lower proximity ratios than $5S^{end}$, corresponding to an increased linker DNA distance. The overall distribution remained well defined, and no peaks corresponding to additional conformations were induced. Acetylated $5S^{end}$ nucleosomes showed a broader distribution of linker arm distances, again extending up to values of $P = 0.7$ as in the case of nonacetylated nucleosomes. The relative fraction of high-FRET conformations, however, is reduced, and more nucleosomes were observed with increased linker arm distances. This is in agreement with observations from ensemble fluorimetry, where an increase of the average linker arm distance was found.[15] As discussed above, the broader distribution for the $5S^{end}$ nucleosomes can probably not be explained by positioning heterogeneity since any such heterogeneity stays constant between samples and does not depend on the label position (Figure 9). We interpret the single molecule data such that acetylation of all histones causes a redistribution between multiple linker DNA conformations present in the ensemble, which, at the time scale of the experiment (few ms), appear as quasi-static components.

In summary, the major effect of histone acetylation occurs on the linker DNA part, where the reduced charge of the tails leads to an opening of the nucleosome structure for both the 601 and 5S sequences. The DNA wrapped around the central part of the octamer was less affected by histone acetylation, which suggests that the electrostatic changes in the tails predominantly influence the interaction with the external parts of the DNA. The details of the DNA sequence itself seem to have only a minor impact in determining the effect of histone acetylation.

Stability of Nucleosomes. Finally, we analyzed how far DNA sequence variation or acetylation of histones alters the intrinsic stability of the nucleosomes. We compared internally labeled nonacetylated 601 and 5S and acetylated 601 nucleosomes at increasing salt concentrations in spFRET by computing the ratio of all FRET- exhibiting bursts to the total number of bursts including the zero-FRET events, which to a large extent arise from free DNA. The experiments were performed under quasi-bulk conditions (addition of 15 nM unlabeled nucleosomes: "+ul") and true single molecule concentrations ("−ul"). The concentration of labeled nucleosomes was 50 pM in all cases. Figure 10 shows the fraction of intact nucleosomes at NaCl concentrations between 5 and 150 mM, normalized to the value at low ionic strength.

5S nucleosomes were more susceptible to salt-induced destabilization than 601 nucleosomes at both 15 nM and 50 pM nucleosome concentrations. This may be linked to the higher conformational flexibility, as indicated by the wider distribution

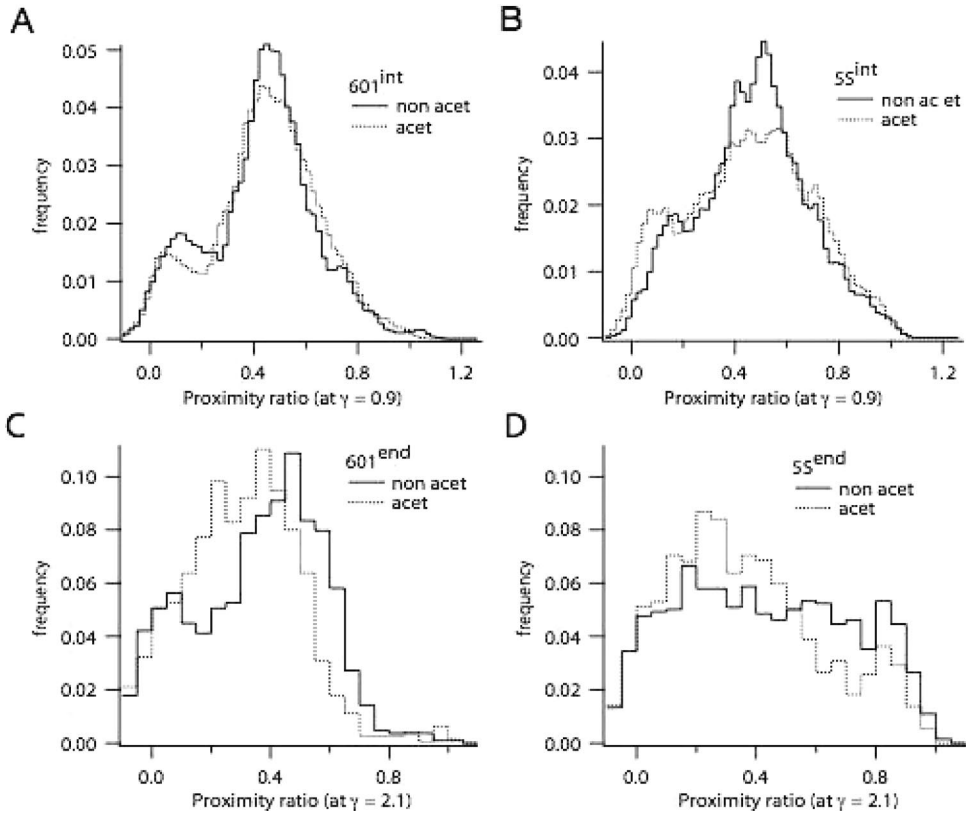

Figure 8. Proximity ratio distributions of acetylated (dotted lines) vs nonacetylated (solid lines) nucleosomes assembled on either the 5S DNA or the 601 fragment. Linker DNA labeled and internally labeled nucleosomes are compared at 100 mM NaCl.

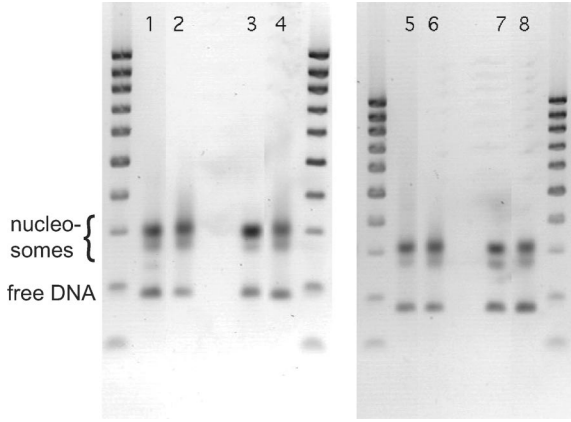

Figure 9. Analysis of reconstituted nucleosome samples by electrophoresis on 2% agarose gels. Left side: end-labeled nucleosomes, 1: 5S, nonacetylated, 2: 5S, acetylated, 3: 601, nonacetylated, 4: 601, acetylated. Right side: internally labeled nucleosomes, 5: 5S, nonacetylated, 6: 5S, acetylated, 7: 601, nonacetylated, 8: 601, acetylated. The unlabeled lanes are DNA marker ladders of multiples of 100 base pairs.

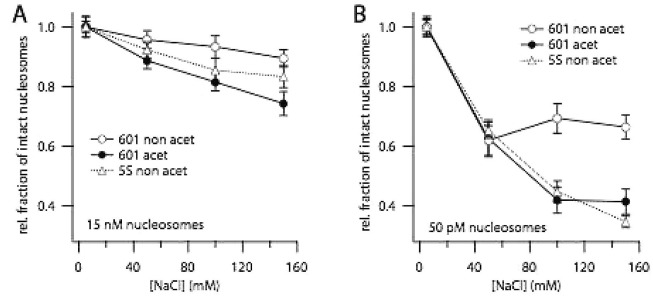

Figure 10. Dependence of nucleosome stability on DNA sequence and histone acetylation measured on internally labeled nucleosomes. (A) Intact nucleosome fraction measured under quasi-bulk conditions (addition of 15 nM unlabeled HeLa nucleosomes to 50 pM labeled sample). (B) Same experiment under single molecule concentrations (no additional unlabeled nucleosomes present). In both cases, histone acetlyation lowers the stability of nucleosomes at elevated salt concentrations.

of the proximity ratios (see Figure 7B). Histone acetylation reduced the stability of 601 nucleosomes. The destabilization under quasi-bulk conditions was even larger than for nonacetylated 5S nucleosomes. At single molecule concentrations, a similar tendency was observed for all constructs, though all nucleosomes suffered from increased dissociation at higher salt levels. Again, nonacetylated 601 nucleosomes were by far more stable than the others. The more open structure of acetylated nucleosomes parallels their increased tendency to dissociate at higher ionic strength. The reason may be that the neutralization of the positive lysine residues decreases the interaction of the tails with the negative phosphate groups of the DNA, and the complex is destabilized. This effect is more pronounced at physiological salt concentrations. Loosening of the nucleosome structure through changing the electrostatic interactions could enable a spontaneous rearrangement of the nucleosomes.

Conclusion

Fluorescence-based assays to monitor structural changes of nucleosomes have gained substantial interest in recent years. Most approaches worked on the ensemble level,[14,15,41−45] but experiments that report on structural changes on the single molecule level are still rare. First results on local unwrapping kinetics were reported,[24,25] in which the nucleosomes were fixed to a surface. While this enabled long-time observations over several seconds, immobilization could also introduce surface-

related artifacts. In our previous work, we established a model system that analyzes the nucleosome conformation free in solution.[27] A confocal microscope is used for single molecule detection at sample concentrations of less than 100 pM. With a similar approach, Kelbauskas et al.[35] recently investigated sequence-specific nucleosome stability, using internally labeled nucleosome constructs comparable to those used in our previous work.

Here we expanded the single molecule analysis of nucleosomes in two ways, which, to our knowledge, have not been addressed so far. First, we introduced the technique of deliberately detuned detection and presented an analysis of the potential increase in separation efficiency for low-FRET peaks in the spFRET histogram. Optimizing detection conditions in this way allowed us to detect for the first time single-pair FRET in linker-DNA-labeled nucleosomes, which due to their low-energy transfer are generally difficult to separate from free DNA present in solution and other zero-FRET species. The combination of information from both linker-DNA and internally labeled DNA sites advances the analysis of structural changes of nucleosomes. The most important result is that here it has been shown for the first time by a direct measurement free in solution that histone acetylation opens the nucleosome structure starting at the linker DNA ends; thus, histone acetylation probably facilitates DNA "unrolling".[45] Second, we use the concentration of unlabeled nucleosomes as an efficient way to control and assess the stability of nucleosome complexes in spFRET measurements. A sufficiently stable nucleosome sample is essential to acquire reliable conformational data at quasi-bulk concentrations. Thus, we can stabilize the sample either by adding unlabeled nucleosomes to bulk concentration while keeping the label concentration in the spFRET range or by lowering the total nucleosome concentration, inducing conditions where the stability of the complexes can be studied and correlated to their conformational heterogeneity.

The interaction between DNA and histone is largely electrostatic, thus salt concentration is a major source for destabilization. High ionic strengths will lead to disruption of the nucleosome. Additionally, the low particle concentrations under 100 pM encountered in single molecule experiments will further promote dissociation. Thus, salt concentration and nucleosome dilution have a similar potential to promote nucleosome dissociation. This aspect was pointed out in bulk experiments by Cotton and Hamkalo using less stable nucleosome sequences,[38] and Gottesfeld and Luger[37] recently determined dissociation constants of less stable positioning sequences to be in the range of 30−60 pM. Their work was based on successive dilution of nucleosomes and subsequent quantification of the dissociated particles in a gel. In a follow up publication, they questioned the reliability of this analysis.[46] Nevertheless, their work supports the idea that single molecule experiments on nucleosome complexes have to face the problem of spontaneous dissociation. Bulk sample or gel techniques, however, involve potential interactions with nearby surfaces or a gel matrix, which potentially contributes to unwanted interactions. Single molecule experiments that analyze nucleosomes in free diffusion do not suffer from these perturbations and define a clean environment for the analysis of the underlying dynamics.

We found that 5S nucleosomes were significantly more destabilized by salt and dilution than nucleosomes of the 601 sequence. Thus, the stability of the complex was directly linked to their affinity to the octamer. Previous biochemical studies showed that different DNA sequences strongly vary in their affinity toward the histone octamer.[28] It is therefore not surprising that less affine sequences like the 5S sequence are more easily dissociated from the histone core by salt concentration and sample dilution than the 601 nucleosomes. Finally, acetylation of all histones also led to a significant destabilization and facilitated dissociation compared to nonacetylated complexes.

The most important effect that we could demonstrate here is the significant shift in FRET populations for the linker-DNA labeled nucleosome samples upon histone acetylation or sequence variation and the absence of such a shift for the internally labeled DNAs. Our earlier bulk experiments indicated a systematic change in average linker distance depending on the ionic environment, linker histone H1 binding, or histone acetylation.[14,15] Here we could show for the first time details of such structural changes by observing nucleosomes free in solution under single molecule conditions. The results suggest that the first parts of the nucleosome that "open up" under conditions where access to nucleosomal DNA is factilitated, such as histone modification, are the linker DNA arms. This result has important consequences for models of protein association to nucleosomal DNA and nucleosome remodeling. Noteworthy, molecular modeling studies of the nucleosome[47,48] indicate the presence of internal modes that facilitate exactly such an opening. Further spFRET studies, in particular using labels on the DNA and the protein core together with advanced methods for data acquisition[49,50] and analysis,[51] will help to elucidate structural details of these mechanisms experimentally.

Acknowledgment. We thank Claus Seidel for inspiring discussions, Jon Widom for generously providing us with nucleosome positioning sequence constructs, and Florian Hauger for establishing sample preparation conditions. This work was supported by a grant from the VW foundation from the program "Physics, Chemistry and Biology with single molecules" and by the DFG research initiative SPP 1128.

References and Notes

(1) Shibata, J. H.; Wilcoxon, J.; Schurr, J. M.; Knauf, V. *Biochemistry* **1984**, *23*, 1188–94.
(2) Pfannschmidt, C.; Langowski, J. *J. Mol. Biol.* **1998**, *275*, 601–11.
(3) Bussiek, M.; Klenin, K.; Langowski, J. *J. Mol. Biol.* **2002**, *322*, 707–18.
(4) van Holde, K. E. *Chromatin*; Springer: Heidelberg, 1989.
(5) Woodcock, C. L.; Grigoryev, S. A.; Horowitz, R. A.; Whitaker, N. *Proc. Natl. Acad. Sci. U.S.A.* **1993**, *90*, 9021–5.
(6) Wedemann, G.; Langowski, J. *Biophys. J.* **2002**, *82*, 2847–59.
(7) Schiessel, H.; Gelbart, W. M.; Bruinsma, R. *Biophys. J.* **2001**, *80*, 1940–56.
(8) Aumann, F.; Lankas, F.; Caudron, M.; Langowski, J. *Phys. Rev. E (Stat., Nonlinear, Soft Matt. Phys.)* **2006**, *73*, 041927.
(9) Wang, J.; Hogan, M.; Austin, R. H. *Proc. Natl. Acad. Sci. U.S.A.* **1982**, *79*, 5896–900.
(10) Schurr, J. M.; Schurr, R. L. *Biopolymers* **1985**, *24*, 1931–40.
(11) Schiessel, H.; Widom, J.; Bruinsma, R. F.; Gelbart, W. M. *Phys. Rev. Lett.* **2001**, *86*, 4414–7.
(12) Fletcher, T. M.; Hansen, J. C. *J. Biol. Chem.* **1995**, *270*, 25359–62.
(13) Clegg, R. M. Fluorescence resonance energy transfer. In *Fluorescence imaging spectroscopy and microscopy*; Wang, X. F., Herman, B. Eds.; John Wiley & Sons: New York, 1996; pp 179−252.
(14) Tóth, K.; Brun, N.; Langowski, J. *Biochemistry* **2001**, *40*, 6921–8.
(15) Tóth, K.; Brun, N.; Langowski, J. *Biochemistry* **2006**, *45*, 1591–8.
(16) Bussiek, M.; Toth, K.; Schwarz, N.; Langowski, J. *Biochemistry* **2006**, *45*, 10838–46.
(17) Schalch, T.; Duda, S.; Sargent, D. F.; Richmond, T. J. *Nature* **2005**, *436*, 138–41.
(18) Bednar, J.; Horowitz, R. A.; Grigoryev, S. A.; Carruthers, L. M.; Hansen, J. C.; Koster, A. J.; Woodcock, C. L. *Proc. Natl. Acad. Sci. U.S.A.* **1998**, *95*, 14173–8.
(19) Ha, T.; Enderle, T.; Ogletree, D. F.; Chemla, D. S.; Selvin, P. R.; Weiss, S. *Proc. Natl. Acad. Sci. U.S.A.* **1996**, *93*, 6264–8.

(20) Jia, Y.; Sytnik, A.; Li, L.; Vladimirov, S.; Cooperman, B. S.; Hochstrasser, R. M. *Proc. Natl. Acad. Sci. U.S.A.* **1997**, *94*, 7932–6.
(21) Deniz, A. A.; Dahan, M.; Grunwell, J. R.; Ha, T.; Faulhaber, A. E.; Chemla, D. S.; Weiss, S.; Schultz, P. G. *Proc. Natl. Acad. Sci. U.S.A.* **1999**, *96*, 3670–5.
(22) Talaga, D. S.; Lau, W. L.; Roder, H.; Tang, J.; Jia, Y.; DeGrado, W. F.; Hochstrasser, R. M. *Proc. Natl. Acad. Sci. U.S.A.* **2000**, *97*, 13021–6.
(23) Schuler, B.; Lipman, E. A.; Eaton, W. A. *Nature* **2002**, *419*, 743–7.
(24) Koopmans, W. J.; Brehm, A.; Logie, C.; Schmidt, T.; van Noort, J. *J. Fluoresc.* **2007**, *17*, 785–95.
(25) Tomschik, M.; Zheng, H.; van Holde, K.; Zlatanova, J.; Leuba, S. H. *Proc. Natl. Acad. Sci. U.S.A.* **2005**, *102*, 3278–83.
(26) Lovullo, D.; Daniel, D.; Yodh, J.; Lohr, D.; Woodbury, N. W. *Anal. Biochem.* **2005**, *341*, 165–72.
(27) Gansen, A.; Hauger, F.; Toth, K.; Langowski, J. *Anal. Biochem.* **2007**, *368*, 193–204.
(28) Thastrom, A.; Lowary, P. T.; Widlund, H. R.; Cao, H.; Kubista, M.; Widom, J. *J. Mol. Biol.* **1999**, *288*, 213–29.
(29) Deniz, A. A.; Laurence, T. A.; Dahan, M.; Chemla, D. S.; Schultz, P. G.; Weiss, S. *Annu. Rev. Phys. Chem.* **2001**, *52*, 233–53.
(30) Hammermann, M.; Toth, K.; Rodemer, C.; Waldeck, W.; May, R. P.; Langowski, J. *Biophys. J.* **2000**, *79*, 584–94.
(31) Wachsmuth, M.; Weidemann, T.; Muller, G.; Hoffmann-Rohrer, U. W.; Knoch, T. A.; Waldeck, W.; Langowski, J. *Biophys. J.* **2003**, *84*, 3353–63.
(32) Weidemann, T.; Wachsmuth, M.; Knoch, T. A.; Muller, G.; Waldeck, W.; Langowski, J. *J. Mol. Biol.* **2003**, *334*, 229–40.
(33) Eggeling, C.; Fries, J. R.; Brand, L.; Gunther, R.; Seidel, C. A. *Proc. Natl. Acad. Sci. U.S.A.* **1998**, *95*, 1556–61.
(34) Enderlein, J.; Goodwin, P. M.; Van Orden, A.; Ambrose, W. P.; Erdmann, R.; Keller, R. A. *Chem. Phys. Lett.* **1997**, *270*, 464–70.
(35) Kelbauskas, L.; Chan, N.; Bash, R.; Debartolo, P.; Sun, J.; Woodbury, N.; Lohr, D. *Biophys. J.* **2008**, *94*, 147−158.
(36) Claudet, C.; Angelov, D.; Bouvet, P.; Dimitrov, S.; Bednar, J. *J. Biol. Chem.* **2005**, *280*, 19958–65.
(37) Gottesfeld, J. M.; Luger, K. *Biochemistry* **2001**, *40*, 10927–33.
(38) Cotton, R. W.; Hamkalo, B. A. *Nucleic Acids Res.* **1981**, *9*, 445–57.
(39) Meersseman, G.; Pennings, S.; Bradbury, E. M. *J. Mol. Biol.* **1991**, *220*, 89–100.
(40) Flaus, A.; Richmond, T. J. *J. Mol. Biol.* **1998**, *275*, 427–41.
(41) Park, Y. J.; Dyer, P. N.; Tremethick, D. J.; Luger, K. *J. Biol. Chem.* **2004**, *279*, 24274–82.
(42) White, C. L.; Luger, K. *J. Mol. Biol.* **2004**, *342*, 1391–402.
(43) Yang, J. G.; Madrid, T. S.; Sevastopoulos, E.; Narlikar, G. J. *Nat. Struct. Mol. Biol.* **2006**, *13*, 1078–83.
(44) Yang, J. G.; Narlikar, G. J. *Methods* **2007**, *41*, 291–5.
(45) Li, G.; Widom, J. *Nat. Struct. Mol. Biol.* **2004**, *11*, 763–9.
(46) Thastrom, A.; Gottesfeld, J. M.; Luger, K.; Widom, J. *Biochemistry* **2004**, *43*, 736–41.
(47) Roccatano, D.; Barthel, A.; Zacharias, M. *Biopolymers* **2007**, *85*, 407–21.
(48) Voltz, K.; Trylska, J.; Tozzini, V.; Kurkal-Siebert, V.; Langowski, J.; Smith, J. *J. Comput. Chem.* **2008**, *29*, 1429−1439.
(49) Lee, N. K.; Kapanidis, A. N.; Wang, Y.; Michalet, X.; Mukhopadhyay, J.; Ebright, R. H.; Weiss, S. *Biophys. J.* **2005**, *88*, 2939–53.
(50) Muller, B. K.; Zaychikov, E.; Brauchle, C.; Lamb, D. C. *Biophys. J.* **2005**, *89*, 3508–22.
(51) Rothwell, P. J.; Berger, S.; Kensch, O.; Felekyan, S.; Antonik, M.; Wohrl, B. M.; Restle, T.; Goody, R. S.; Seidel, C. A. *Proc. Natl. Acad. Sci. U.S.A.* **2003**, *100*, 1655–60.

JP7114737